



Measurement of the time-integrated CP asymmetry in $D^0 \rightarrow K_S^0 K_S^0$ decays

LHCb collaboration[†]

Abstract

A measurement of the time-integrated CP asymmetry in $D^0 \rightarrow K_S^0 K_S^0$ decays is reported. The data correspond to an integrated luminosity of about 2 fb^{-1} collected in 2015–2016 by the LHCb collaboration in pp collisions at a centre-of-mass energy of 13 TeV. The D^0 candidate is required to originate from a $D^{*+} \rightarrow D^0 \pi^+$ decay, allowing the determination of the flavour of the D^0 meson using the pion charge. The $D^0 \rightarrow K^+ K^-$ decay, which has a well measured CP asymmetry, is used as a calibration channel. The CP asymmetry for $D^0 \rightarrow K_S^0 K_S^0$ is measured to be

$$\mathcal{A}^{CP}(D^0 \rightarrow K_S^0 K_S^0) = (4.3 \pm 3.4 \pm 1.0)\%,$$

where the first uncertainty is statistical and the second is systematic. This result is combined with the previous LHCb measurement at lower centre-of-mass energies to obtain

$$\mathcal{A}^{CP}(D^0 \rightarrow K_S^0 K_S^0) = (2.3 \pm 2.8 \pm 0.9)\%.$$

Published in JHEP 11 (2018) 048

© 2018 CERN for the benefit of the LHCb collaboration. CC-BY-4.0 licence.

[†]Authors are listed at the end of this paper.

1 Introduction

In the Standard Model, violation of charge-parity (CP) symmetry originates from the presence of a single phase in the Cabibbo-Kobayashi-Maskawa (CKM) matrix [1]. Experimental results support the CKM mechanism for CP violation, but additional sources of CP violation are needed to explain cosmological observations of the relative abundance of matter and antimatter in the universe [2]. In the charm sector, CP violation has not yet been observed, but measurements of CP asymmetries in Cabibbo-suppressed $D^0 \rightarrow h^+h^-$ decays ($h = \pi, K$) have reached 0.2% and 0.03% precision for time-integrated [3] and indirect CP asymmetries [4], respectively.

The $D^0 \rightarrow K_s^0 K_s^0$ decay is a promising discovery channel for CP violation in charm decays [5]. Only loop-suppressed amplitudes and exchange diagrams that vanish in the SU(3) flavour limit contribute to this decay. These amplitudes can have different strong and weak phases and are of similar size. The time-integrated CP asymmetry, \mathcal{A}^{CP} , in $D^0 \rightarrow K_s^0 K_s^0$ decays may therefore be enhanced to an observable level [6], and could be as large as 1.1% [5]. Examples of such diagrams are shown in Fig. 1. The most precise measurement of this asymmetry to date, $\mathcal{A}^{CP}(K_s^0 K_s^0) = (-0.02 \pm 1.53 \pm 0.17)\%$, has been performed by the Belle collaboration [7]. Earlier measurements were also performed by the LHCb [8] and CLEO [9] collaborations. This article reports a new measurement of \mathcal{A}^{CP} in the decay $D^0 \rightarrow K_s^0 K_s^0$ using LHCb data collected in 2015 and 2016.

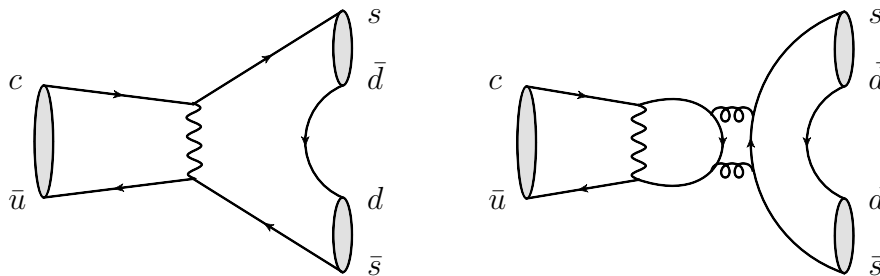


Figure 1: Exchange (left) and penguin annihilation (right) diagrams contributing to the $D^0 \rightarrow K_s^0 K_s^0$ amplitude. Based on Ref. [5].

The measurement of the CP asymmetry, defined as

$$\mathcal{A}^{CP}(K_s^0 K_s^0) \equiv \frac{\Gamma(D^0 \rightarrow K_s^0 K_s^0) - \Gamma(\bar{D}^0 \rightarrow K_s^0 K_s^0)}{\Gamma(D^0 \rightarrow K_s^0 K_s^0) + \Gamma(\bar{D}^0 \rightarrow K_s^0 K_s^0)}, \quad (1)$$

requires knowledge of the flavour of the D^0 meson at production. A sample of flavour-tagged $D^0 \rightarrow K_s^0 K_s^0$ decays is obtained by selecting D^{*+} mesons that are produced in the primary interaction (hereafter referred to as prompt), with the subsequent decay $D^{*+} \rightarrow D^0 \pi^+$.¹ The charge of the pion in this decay identifies the flavour of the accompanying D^0 meson. The effect of $D^0 - \bar{D}^0$ mixing [10] is negligible compared to the precision of this analysis and is not considered further.

The experimentally measured quantity is the raw asymmetry, defined as

$$\mathcal{A}^{\text{raw}} \equiv \frac{N_{D^0} - N_{\bar{D}^0}}{N_{D^0} + N_{\bar{D}^0}}, \quad (2)$$

¹The inclusion of charge-conjugate processes is implied throughout this document, unless explicitly specified.

where N_{D^0} is the measured yield of $D^{*+} \rightarrow D^0\pi^+$, $D^0 \rightarrow K_s^0 K_s^0$ decays and $N_{\bar{D}^0}$ is the measured yield of $D^{*-} \rightarrow \bar{D}^0\pi^-$, $\bar{D}^0 \rightarrow K_s^0 K_s^0$ decays. This observable is related to the CP asymmetry by the expression, valid for small asymmetries,

$$\mathcal{A}^{\text{raw}} \approx \mathcal{A}^{CP} + \mathcal{A}^{\text{prod}} + \mathcal{A}^{\text{det}}, \quad (3)$$

where $\mathcal{A}^{\text{prod}}$ is the $D^{*\pm}$ production asymmetry, defined as $\mathcal{A}^{\text{prod}} \equiv \frac{\sigma(D^{*+}) - \sigma(D^{*-})}{\sigma(D^{*+}) + \sigma(D^{*-})}$, and \mathcal{A}^{det} is the π_{tag}^\pm detection asymmetry, defined as $\mathcal{A}^{\text{det}} \equiv \frac{\epsilon(\pi_{\text{tag}}^+) - \epsilon(\pi_{\text{tag}}^-)}{\epsilon(\pi_{\text{tag}}^+) + \epsilon(\pi_{\text{tag}}^-)}$. The symbol π_{tag}^\pm refers to the pion in the $D^{*\pm}$ decay. To a very good approximation, knowledge of \mathcal{A}^{det} and $\mathcal{A}^{\text{prod}}$ is unnecessary when using a calibration channel with the same production and tagging mechanism. The decay channel $D^0 \rightarrow K^+ K^-$ is used for this purpose. The production and detection asymmetries cancel when taking the difference of the raw asymmetries:

$$\Delta\mathcal{A}^{CP} \equiv \mathcal{A}^{\text{raw}}(K_s^0 K_s^0) - \mathcal{A}^{\text{raw}}(K^+ K^-) \quad (4)$$

$$= \mathcal{A}^{CP}(K_s^0 K_s^0) - \mathcal{A}^{CP}(K^+ K^-). \quad (5)$$

The quantity $\mathcal{A}^{CP}(K^+ K^-)$ has been measured with a precision of 0.2% [3], thus allowing the determination of $\mathcal{A}^{CP}(K_s^0 K_s^0)$.

2 LHCb detector

The LHCb detector [11, 12] is a single-arm forward spectrometer covering the pseudorapidity range $2 < \eta < 5$, designed for the study of particles containing b or c quarks. The detector includes a high-precision tracking system consisting of a silicon-strip vertex detector surrounding the pp interaction region, a large-area silicon-strip detector (TT) located upstream of a dipole magnet with a bending power of about 4 Tm, and three stations of silicon-strip detectors and straw drift tubes placed downstream of the magnet. The tracking system provides a measurement of momentum, p , of charged particles with a relative uncertainty that varies from 0.5% at low momentum to 1.0% at 200 GeV/ c . The minimum distance of a track to a primary vertex (PV), the impact parameter (IP), is measured with a resolution of $(15 + 29/p_T) \mu\text{m}$, where p_T is the component of the momentum transverse to the beam, in GeV/ c . Different types of charged hadrons are distinguished using information from two ring-imaging Cherenkov (RICH) detectors. Photons, electrons and hadrons are identified by a calorimeter system consisting of scintillating-pad and preshower detectors, an electromagnetic calorimeter and a hadronic calorimeter. Muons are identified by a system composed of alternating layers of iron and multiwire proportional chambers. The magnetic field deflects oppositely-charged particles in opposite directions and this can lead to detection asymmetries. Periodically reversing the magnetic field polarity throughout the data taking almost cancels the effect. The configuration with the magnetic field pointing upwards (downwards), MagUp (MagDown), bends positively (negatively) charged particles in the horizontal plane towards the centre of the LHC ring.

The online event selection is performed by a trigger, which consists of a hardware stage, based on information from the calorimeter and muon systems, followed by a software stage, which applies a full event reconstruction. At the hardware trigger stage, events are required to have a muon with high p_T or a hadron, photon or electron with high transverse-energy deposit in the calorimeters.

Simulated events are used at various phases of the analysis. In the simulation, pp collisions are generated using PYTHIA [13] with a specific LHCb configuration [14]. Decays of hadronic particles are described by EVTGEN [15], in which final-state radiation is generated using PHOTOS [16]. The interaction of the generated particles with the detector, and its response, are implemented using the GEANT4 toolkit [17] as described in Ref. [18].

3 Event selection

The 2015 and 2016 data samples collected in pp collisions at 13 TeV, which correspond to about 2fb^{-1} of integrated luminosity, are used in this analysis. Candidates are reconstructed in the decay $D^{*+} \rightarrow D^0\pi^+$, followed by $D^0 \rightarrow K_s^0 K_s^0$ and then $K_s^0 \rightarrow \pi^+\pi^-$. The hardware trigger decision is required to be based either on the transverse energy deposited in the hadronic calorimeter by a charged particle from the decay of the D^0 meson, or on signatures not associated with the D^{*+} decay, such as a high- p_T muon, or a high transverse-energy deposit in the electromagnetic or hadronic calorimeters. The first stage of the software trigger selects a sample with enhanced heavy-flavour content by requiring the presence of a large IP, high- p_T charged particle. In the second stage of the software trigger, each selected event is required to contain at least one fully-reconstructed candidate for the $D^{*+} \rightarrow D^0\pi^+$, $D^0 \rightarrow K_s^0 K_s^0$ decay.

The decays $K_s^0 \rightarrow \pi^+\pi^-$ are reconstructed in two different categories: the first involving K_s^0 mesons that decay early enough for the decay products to be reconstructed in the vertex detector; and the second containing K_s^0 candidates that decay outside the acceptance of the vertex detector, but within the TT acceptance. These categories are referred to as *long* and *downstream*, respectively. The long category has better mass, momentum and decay-vertex resolution than the downstream category. In this analysis at least one K_s^0 in each D^0 decay is required to be of the long type. There are therefore two subsamples used: one where both K_s^0 candidates are long and the other where one is long and the other is downstream. These are referred to as the LL and LD subsamples, and are analysed separately, since they exhibit different resolutions. One or more of the charged decay products from a long K_s^0 meson is required to activate the first stage of the software trigger. The pion candidates used in the K_s^0 reconstruction are required to be high-quality tracks, using the χ^2/ndf of the track fit and the output $\mathcal{P}_{\text{fake}}$ of a multivariate classifier, trained to identify fake tracks, that combines information from the particle identification and tracking systems. To ensure that pion candidates do not originate from the PV, they are required to satisfy $\chi_{\text{IP}}^2 > 36$. The quantity χ_{IP}^2 for a given particle is defined as the difference in the vertex fit χ^2 of the PV associated to the particle, reconstructed with and without the particle being considered. For downstream K_s^0 candidates, the pions are required to satisfy $p > 3\text{ GeV}/c$ and $p_T > 175\text{ MeV}/c$.

Two oppositely charged pions are used to form K_s^0 candidates. The vertex fit is required to satisfy $\chi^2 < 30$ and the χ_{IP}^2 is required to be greater than 9 (4) for long (downstream) K_s^0 candidates. Furthermore, long (downstream) K_s^0 candidates are required to satisfy $p_T > 500$ (750) MeV/c .

Two reconstructed K_s^0 candidates are paired to form D^0 candidates, requiring $\chi^2 < 10$ for the vertex fit. The sum of the p_T of the K_s^0 candidates is required to exceed 1500 (2000) MeV/c for LL (LD) candidates. The angle between the D^0 momentum and the vector connecting the PV to the D^0 decay vertex is required to be less than 34.6 mrad.

The measured decay time of the D^0 meson is required to be greater than 0.2 ps. Finally, the D^0 mass is required to be within 20 MeV/ c^2 of the known value [10].

A pion candidate (π_{tag}^+) is added to a reconstructed D^0 meson to form a D^{*+} candidate, with a D^{*+} vertex fit which is required to have $\chi^2 < 25$. The π_{tag}^+ candidate is required to have $p_T > 100$ MeV/ c , and to pass through regions of the detector that are known to have a small detector asymmetry [8]. A small fraction of π_{tag}^\pm candidates are reconstructed with the wrong charge assignment, and are removed by a selection on track quality.

An important source of background is due to the presence of $D^0 \rightarrow K_S^0 \pi^+ \pi^-$ decays, where the $\pi^+ \pi^-$ pair satisfies the K_S^0 selection. In principle, the contribution of this channel can be substantial, due to its large branching fraction, but it is effectively reduced by placing a requirement on the K_S^0 flight distance (FD) and on the mass of the K_S^0 candidates. The quantity χ_{FD}^2 is the square of the measured K_S^0 flight distance divided by the square of its uncertainty. Figure 2 shows a two-dimensional plot of the value of the quantity $\log \chi_{\text{FD}}^2$ for K_S^0 pairs in the LL sample. In the figure, four separate regions are visible. The upper right part of the plot, where both K_S^0 candidates have significant flight distances, is the $D^0 \rightarrow K_S^0 K_S^0$ signal, while the upper left and lower right regions correspond to $D^0 \rightarrow K_S^0 \pi^+ \pi^-$ decays. The lower left is populated by $D^0 \rightarrow \pi^+ \pi^- \pi^+ \pi^-$ decays and combinatorial background. A requirement on χ_{FD}^2 is only necessary for long K_S^0 candidates, since downstream K_S^0 candidates decay far from the PV by construction. For the LL subsample the requirement on the two K_S^0 candidates (K_{S1}^0 and K_{S2}^0) is

$$[\log \chi_{\text{FD}}^2(K_{S1}^0) - 10]^2 + [\log \chi_{\text{FD}}^2(K_{S2}^0) - 10]^2 < 16, \quad (6)$$

while for the LD sample $\log \chi_{\text{FD}}^2(K_{S1}^0) > 2.5$ is imposed on the long K_S^0 candidate.

The K_S^0 mass requirements are

$$\sqrt{[m(K_{S1}^0) - m_{K^0}]^2 + [m(K_{S2}^0) - m_{K^0}]^2} < 10.5 \text{ MeV}/c^2, \quad (7)$$

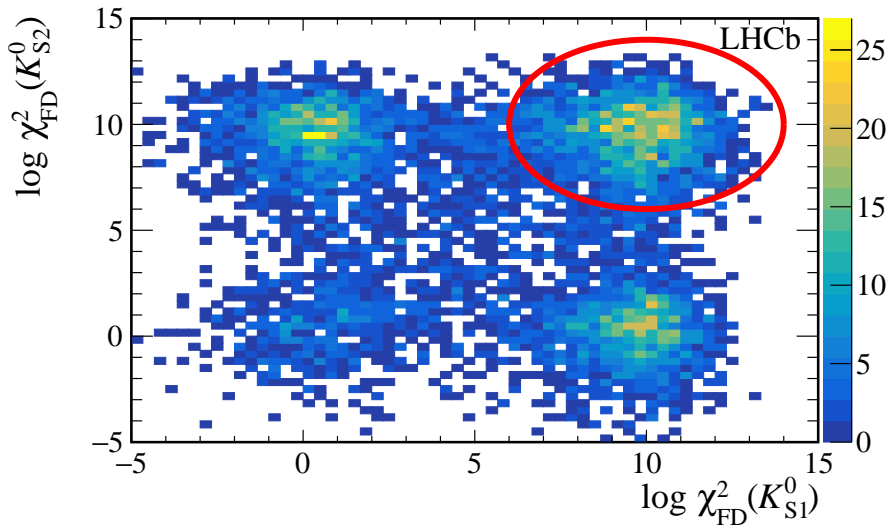


Figure 2: Two-dimensional distribution of the logarithm of the K_S^0 flight distance significance ($\log \chi_{\text{FD}}^2$) for the two K_S^0 candidates in the LL subsample of $D^0 \rightarrow K_S^0 K_S^0$ decays. The $D^0 \rightarrow K_S^0 K_S^0$ signal can be observed in the upper right region of the plot. The contour corresponds to Eq. 6.

for LL candidates, with $m_{K^0} = 497.6 \text{ MeV}/c^2$ [10], and

$$\sqrt{\left[\frac{m(K_{\text{SL}}^0) - m_{K^0}}{10.5 \text{ MeV}/c^2}\right]^2 + \left[\frac{m(K_{\text{SD}}^0) - m_{K^0}}{15 \text{ MeV}/c^2}\right]^2} < 1, \quad (8)$$

for LD candidates. This selection takes into account the difference in resolution between $m(K_{\text{SL}}^0)$ and $m(K_{\text{SD}}^0)$. The $\log \chi_{\text{FD}}^2(K_{\text{S}}^0)$ and $m(K_{\text{S}}^0)$ regions corresponding to signal and peaking-background candidates are identified using simulations. They are further optimised on charge-integrated data by minimising the expected statistical uncertainty on \mathcal{A}^{raw} .

Events in which the D^{*+} meson is not produced in the primary interaction, but instead is the product of a b -hadron decay, are characterised by a different production asymmetry and are treated as background. These so-called secondary D^{*+} candidates tend to have larger values of $\chi_{\text{IP}}^2(D^0)$ than prompt D^{*+} candidates and are suppressed by requiring $\log \chi_{\text{IP}}^2(D^0) < 3.0$ (3.5) for the LL (LD) subsample. The requirement $\log \chi_{\text{IP}}^2(\pi_{\text{tag}}^+) < 2.5$ is imposed on both subsamples. Simulated events are used to estimate the residual secondary fraction in the LL and LD subsamples to be 9% and 13%, respectively.

A multivariate classifier, based on the k -nearest neighbours (kNN) algorithm [19], is used to further suppress combinatorial background. The kNN algorithm classifies events according to the fraction of signal events among its k nearest neighbours (taken from the training sample of signal and background events), where the distance is calculated in the n -dimensional space of the input variables and k is a positive integer. The training sample uses simulated events for the signal and data events from the D^0 mass sidebands for the background. A wide range of input variables based on track and vertex quality, the transverse momenta of K_{S}^0 and D^0 candidates, helicity angles of the K_{S}^0 and D^0 decays and particle identification information on the pions in the D^0 decays was initially considered. Variables depending on the π_{tag}^{\pm} track are not included in the classifier to avoid introducing possible bias on the asymmetry measurement. The actual variables used, the value of k , and the selection on the classifier output are optimised separately for the LL and LD subsamples, using the expected statistical uncertainty on the raw asymmetry as a figure of merit.

For the $D^0 \rightarrow K^+K^-$ control channel, an attempt is made to keep the selection similar to the $D^0 \rightarrow K_{\text{S}}^0K_{\text{S}}^0$ channel, although some selections made at the software trigger level are different for the two channels. Charged tracks positively identified as kaons in the RICH detectors are selected to reconstruct D^0 candidates. The kaons are required to satisfy $\chi_{\text{IP}}^2 > 4$. For the D^0 candidates, at least one of the kaons is required to have $p_{\text{T}} > 1 \text{ GeV}/c$. The sum of the kaon momenta is required to exceed $5 \text{ GeV}/c$ and the D^0 p_{T} is required to be at least $1 \text{ GeV}/c$. Furthermore, the angle between the D^0 momentum vector and the vector connecting the primary and decay vertices is required to be less than 17.3 mrad . The following selections are the same as for the $D^0 \rightarrow K_{\text{S}}^0K_{\text{S}}^0$ channel: π_{tag}^{\pm} fiducial cuts, fake-track probability and χ_{IP}^2 selection; and requirements on D^0 χ_{IP}^2 and invariant mass.

4 Asymmetry measurement

The raw asymmetry for $D^0 \rightarrow K_{\text{S}}^0K_{\text{S}}^0$ is determined by separating the selected candidates into subsets tagged by positively and negatively charged pions. A simultaneous unbinned

maximum likelihood fit to their Δm distributions is performed, where Δm is the difference of the reconstructed invariant mass of the D^{*+} and the D^0 candidates. The calculation of Δm is made after the full decay chain has been reconstructed using a mass constraint on the K_S^0 candidates and constraining the D^{*+} candidate to originate from the PV.

The signal shape is modelled using the Johnson S_U distribution [20], which consists of a core Gaussian-like shape but allows for an asymmetric tail

$$S(x; \mu, \sigma, \delta, \gamma) \propto \left[1 + \left(\frac{x - \mu}{\sigma} \right)^2 \right]^{-\frac{1}{2}} \times \exp \left\{ -\frac{1}{2} \left[\gamma + \delta \sinh^{-1} \left(\frac{x - \mu}{\sigma} \right) \right]^2 \right\}. \quad (9)$$

The background shape is described with an exponential function multiplied by a threshold factor and is zero below a fixed endpoint, which is set to the pion mass m_π

$$B(x; m_\pi, \chi) \propto \sqrt{x - m_\pi} \times \exp \left(\chi \frac{x}{m_\pi} \right). \quad (10)$$

The likelihood function is parametrised in terms of \mathcal{A}^{CP} and the expected total number of events $N_{\text{exp}} = n_{\text{sig}} + n_{\text{bkg}}$

$$\mathcal{L} = \frac{e^{-N_{\text{exp}}}}{N_{\text{obs}}!} \prod_i \left[n_{\text{sig}} \frac{1 + q_i \mathcal{A}_{\text{sig}}^{\text{raw}}}{2} S(\Delta m) + n_{\text{bkg}} \frac{1 + q_i \mathcal{A}_{\text{bkg}}^{\text{raw}}}{2} B_{q_i}(\Delta m) \right], \quad (11)$$

where n_{sig} and n_{bkg} are the signal and background yields, respectively, and the parameter $q_i = \pm 1$ is the charge of the $D^{*\pm}$ candidate and N_{obs} is the total number of candidates. The signal raw asymmetry $\mathcal{A}_{\text{sig}}^{\text{raw}}$ is a free parameter in the fit. The free parameter $\mathcal{A}_{\text{bkg}}^{\text{raw}}$ allows for a possible asymmetry in the combinatorial background. The four parameters in Eq. 9 defining the signal probability distribution function (PDF) are common to the D^{*+} and D^{*-} samples, while the parameter describing the background shape is allowed to differ between the two subsamples. For the LL sample, there are ten free parameters. To achieve convergence of the fit in the smaller LD sample, it is necessary to fix the two parameters that describe the asymmetric tail in the signal PDF to the values obtained from the charge-integrated LL subsample. Based on studies of simulated events, the tail parameters of the LL and LD subsamples are expected to be compatible. Separate fits are performed for the two magnet polarities.

Table 1 shows the results of the simultaneous fits to the $D^0 \rightarrow K_S^0 K_S^0$ candidates. The results on each subset of the data are compatible with each other. The fit is shown in Fig. 3 for the samples collected with the MagUp magnetic field configuration.

For the $D^0 \rightarrow K^+ K^-$ channel, binned χ^2 fits are performed to the Δm distributions of the positively and negatively tagged D^0 decays. The sample consists of 8.25×10^5 selected candidates for the MagDown magnet polarity and 5.61×10^5 candidates for the MagUp magnet polarity. The signal is modelled with a Johnson S_U distribution plus a Gaussian distribution, while the background shape is described by a fourth-degree polynomial multiplied by a $\sqrt{\Delta m - m_\pi}$ threshold factor. There are 12 free parameters, and 150 bins, in each Δm fit. The χ^2 probabilities associated to the fits are 28% (20%) for the negatively (positively) tagged D^0 decays, and 23% (3%) for the negatively (positively) tagged D^0 decays, in the MagUp and MagDown magnet polarities, respectively. Figure 4 shows the results for the MagUp magnet polarity fit. The results obtained for the two

Table 1: Fit results on the $D^0 \rightarrow K_S^0 K_S^0$ LL and LD samples for each magnet polarity, where N_{obs} represents the number of candidates fitted. The purity is determined in the range $144.5 < \Delta m < 146.5 \text{ MeV}/c^2$. For each sample, a χ^2 test statistic for the fitted model and binned data for positively and negatively charged candidates is constructed. The quantity \mathcal{P}_{fit} is the probability of observing a χ^2 value greater than that observed in the fit to real data, determined using simulated pseudoexperiments sampled from the fitted model.

	$\mathcal{A}_{\text{sig}}^{\text{raw}}$	n_{sig}	$\mathcal{A}_{\text{bkg}}^{\text{raw}}$	Purity	$\mathcal{P}_{\text{fit}}(\%)$	N_{obs}
LL MagUp	0.008 ± 0.057	346 ± 21	-0.097 ± 0.069	0.92	48	589
LL MagDown	0.103 ± 0.052	413 ± 24	-0.098 ± 0.068	0.92	43	675
LD MagUp	-0.046 ± 0.102	156 ± 18	-0.021 ± 0.044	0.67	93	758
LD MagDown	-0.078 ± 0.107	152 ± 19	-0.040 ± 0.038	0.60	14	950

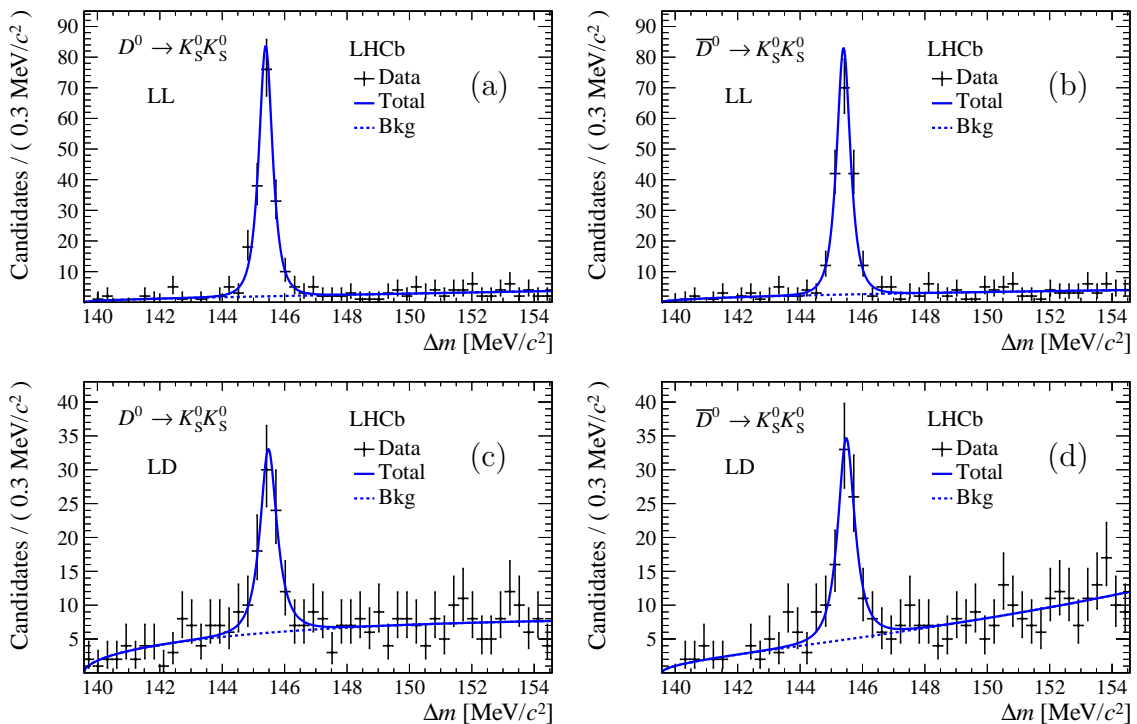


Figure 3: Results of fits to Δm distributions of $D^0 \rightarrow K_S^0 K_S^0$ candidates for MagUp magnet polarity. The fit to (a) $D^{*+} \rightarrow D^0 \pi^+$ and (b) $D^{*-} \rightarrow D^0 \pi^-$ candidates for the LL sample and the fit to (c) $D^{*+} \rightarrow D^0 \pi^+$ and (d) $D^{*-} \rightarrow \bar{D}^0 \pi^-$ candidates for the LD sample are shown. The black crosses represent the data points, the solid blue curve is the total fit function, and the dashed blue curve is the background component of the fit.

magnet polarities are

$$\begin{aligned} \mathcal{A}^{\text{raw}}(K^+ K^-)_{\text{MagUp}} &= -0.0188 \pm 0.0020, \\ \mathcal{A}^{\text{raw}}(K^+ K^-)_{\text{MagDown}} &= 0.0030 \pm 0.0017, \end{aligned} \quad (12)$$

where the uncertainties are statistical. The difference in the MagUp and MagDown values of $\mathcal{A}^{\text{raw}}(K^+ K^-)$ is an indication of a significant π_{tag}^\pm detection asymmetry, which depends on the magnetic field orientation.

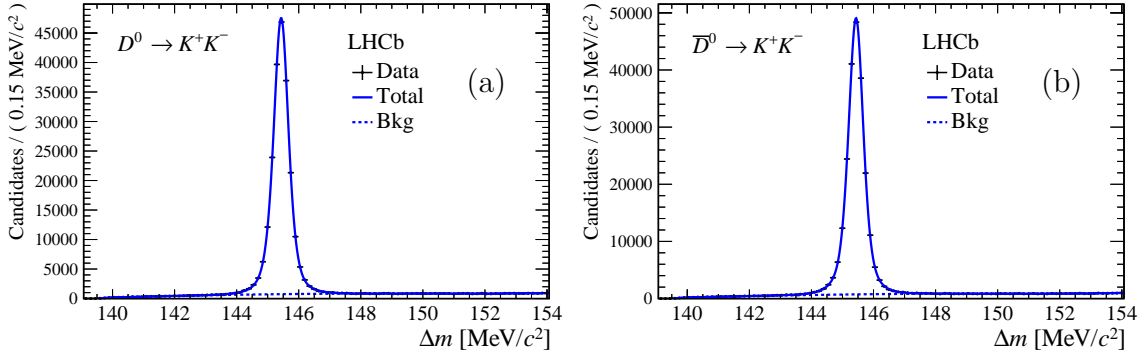


Figure 4: Results of fits to Δm distributions of $D^0 \rightarrow K^+K^-$ candidates for the MagUp magnet polarity. The fits to (a) $D^{*+} \rightarrow D^0\pi^+$ candidates and (b) $D^{*-} \rightarrow \bar{D}^0\pi^-$ candidates are shown. The black points represent the data, the dashed blue and solid blue curves represent the background component and the total fit function, respectively.

5 Systematic uncertainties

The main source of systematic uncertainty arises from the determination of \mathcal{A}^{raw} on the $D^0 \rightarrow K_s^0 K_s^0$ sample. Possible bias in the fitting procedure is evaluated using simulated pseudoexperiments. In particular, the uncertainty related to the choice of the signal model is evaluated by using the nominal model to fit samples generated with two alternative models for the signal PDF: either a sum of two Gaussians with a common mean (for the LL sample) or a single Gaussian (for the LD sample). The background PDF is varied by modifying its behaviour at threshold. Systematic uncertainties of 5×10^{-3} and 0.01 for the LL and LD samples, respectively, are assigned based on this study. As a cross-check, the background shapes are constrained to be the same for the D^{*+} and D^{*-} samples, and the resulting asymmetry is compatible with the nominal. For the $D^0 \rightarrow K^+K^-$ fit, an alternative procedure is used to evaluate the systematic uncertainty associated with the signal PDF. In this case, the signal region ($\pm 2.5 \text{ MeV}/c^2$ around the signal mean) is excluded and only the background shape is fit. The yield is then determined by estimating the background in the signal region by interpolating the fitted background function. Additionally, alternative background shapes are tried, varying the degree of the polynomial. Based on these studies a systematic uncertainty of 2×10^{-3} is assigned to $\mathcal{A}^{\text{raw}}(K^+K^-)$.

The contribution of the residual background of $D^0 \rightarrow K_s^0\pi^+\pi^-$ decays to the fitted LL and LD signal yields is estimated to be $(3.5 \pm 0.7)\%$ and $(5.5 \pm 4.6)\%$, respectively. These values are combined with the $K_s^0\pi^+\pi^-$ background asymmetry, determined from background-dominated regions of the χ_{FD}^2 distributions, to estimate contributions to the systematic uncertainty of 4×10^{-3} and 5×10^{-3} , for the LL and LD samples. Another contribution comes from the residual fraction of secondary decays, which leads to a systematic uncertainty for this source of 2×10^{-3} and 3×10^{-3} for the LL and LD samples. In this case an upper limit of 0.02 for the maximum difference in the production asymmetries of $D^{*\pm}$ mesons and b -hadrons is assumed [21–23].

Potential trigger biases are studied using tagged $D^0 \rightarrow K^+K^-$ decays, by comparing the raw asymmetries obtained in the subsample in which the trigger decision is based on the charged particles from the decay of the D^0 meson, and in the subsample in which

Table 2: Systematic uncertainties on the quantities \mathcal{A}^{raw} and $\Delta\mathcal{A}^{CP}$. The total systematic uncertainties in the last row are obtained by summing the corresponding contributions in each column in quadrature. Uncertainties are expressed in units of 10^{-3} .

Source	$\mathcal{A}^{\text{raw}}(\text{LL})$	$\mathcal{A}^{\text{raw}}(\text{LD})$	$\Delta\mathcal{A}^{CP}(\text{LL})$	$\Delta\mathcal{A}^{CP}(\text{LD})$
Fit procedure	5	10	5	10
$K_s^0\pi^+\pi^-$ background	4	5	4	5
Secondaries	2	3	2	3
Wrong π_{tag}^\pm charge	2	2	–	–
Trigger selection	5	5	5	5
K^+K^- fit procedure	–	–	2	2
Residual detection asymmetry	–	–	2	2
Total	9	13	9	13

the trigger decision is not associated with the D^{*+} decay. The sum in quadrature of the difference (albeit not statistically significant) and of its statistical uncertainty is assigned as a systematic uncertainty, which accounts for residual trigger-induced biases in the difference of measured asymmetries for signal and control channels. This uncertainty amounts to 5×10^{-3} for both the LL and LD samples. The small probability of assigning the wrong charge to the π_{tag}^\pm candidate results in a systematic uncertainty of 2×10^{-3} for both the LL and LD samples. This is obtained by varying the selection on the $\mathcal{P}_{\text{fake}}$ value of π_{tag}^\pm candidates. This uncertainty cancels for $\Delta\mathcal{A}^{CP}$. For each neutral kaon in the final state, asymmetries arising from regeneration and from mixing and CP violation in the $K^0 - \bar{K}^0$ system are suppressed at the $\mathcal{O}(10^{-3})$ level [24]. Since they are expected to affect $D^0 \rightarrow K_s^0 K_s^0$ and $\bar{D}^0 \rightarrow K_s^0 K_s^0$ decays by the same amount, they cancel in \mathcal{A}^{raw} and therefore do not contribute to the systematic uncertainty.

The cancellation of the production and detection asymmetries in the computation of $\Delta\mathcal{A}^{CP}$ may not be perfect due to differences in the kinematics of the $D^0 \rightarrow K_s^0 K_s^0$ candidates and the $D^0 \rightarrow K^+ K^-$ candidates. The offline selection of the two channels aims to keep the kinematics as similar as possible, but the different trigger selections on the final states can introduce differences. The associated systematic uncertainty is evaluated by considering four kinematic variables: the transverse momentum and the pseudorapidity of the D^{*+} candidate and the π_{tag}^+ candidate, respectively. For each variable a one-dimensional weighting is performed on the $D^0 \rightarrow K^+ K^-$ events such that they have the same distribution as the $D^0 \rightarrow K_s^0 K_s^0$ sample. Then $\mathcal{A}^{\text{raw}}(K^+ K^-)$ is determined from the weighted sample. This is repeated for each of the four kinematic variables. The largest change in $\mathcal{A}^{\text{raw}}(K^+ K^-)$ is taken as the systematic uncertainty and this is found to be 2×10^{-3} for both the LL and LD samples. The systematic uncertainties are summarised in Table 2.

6 Results

The procedure described in Sect. 1 is used to combine the results for the raw asymmetries to obtain $\mathcal{A}^{CP}(K_s^0 K_s^0)$ for each of the LL and LD subsamples. For each of the subsamples,

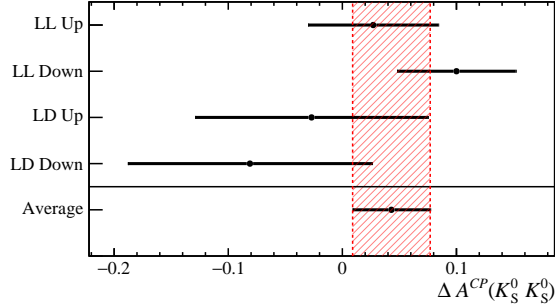


Figure 5: Values of $\Delta\mathcal{A}^{CP}$ obtained for both magnet polarities on the LL and LD samples, along with the average of these measurements. Only statistical uncertainties are shown.

the difference $\Delta\mathcal{A}^{CP}$ is calculated separately for the different magnet polarities using the fitted values of \mathcal{A}^{raw} (Table 1 and Eq. 12). The values of $\Delta\mathcal{A}^{CP}$ corresponding to the two magnet polarities, which are found to be in good agreement (Fig. 5), are averaged by weighting with their statistical uncertainties. The systematic uncertainties are taken from Table 2. Using the LHCb measurement of $\mathcal{A}^{CP}(K^+K^-) = (0.04 \pm 0.12 \pm 0.10)\%$ [3] results in

$$\begin{aligned}\mathcal{A}^{CP}(\text{LL}) &= 0.067 \pm 0.038 \pm 0.009, \\ \mathcal{A}^{CP}(\text{LD}) &= -0.053 \pm 0.074 \pm 0.013,\end{aligned}$$

where the first uncertainty is statistical and the second is systematic. These results are combined by performing an average weighted by the total uncertainties and assuming that the systematic uncertainties are fully correlated. The final result is

$$\mathcal{A}^{CP}(K_S^0 K_S^0) = 0.043 \pm 0.034 \pm 0.010.$$

This measurement is systematically independent of the LHCb Run 1 measurement, $\mathcal{A}^{CP}(K_S^0 K_S^0) = -0.029 \pm 0.052 \pm 0.022$ [8], and is compatible with it. An average, weighted by the total uncertainties, of the two measurements is performed to obtain

$$\mathcal{A}^{CP}(K_S^0 K_S^0) = 0.023 \pm 0.028 \pm 0.009.$$

These results are compatible with the expectations of the Standard Model [5] and with previous measurements [7, 9].

Acknowledgements

We express our gratitude to our colleagues in the CERN accelerator departments for the excellent performance of the LHC. We thank the technical and administrative staff at the LHCb institutes. We acknowledge support from CERN and from the national agencies: CAPES, CNPq, FAPERJ and FINEP (Brazil); MOST and NSFC (China); CNRS/IN2P3 (France); BMBF, DFG and MPG (Germany); INFN (Italy); NWO (Netherlands); MNiSW and NCN (Poland); MEN/IFA (Romania); MinES and FASO (Russia); MinECo (Spain); SNSF and SER (Switzerland); NASU (Ukraine); STFC (United Kingdom); NSF (USA). We acknowledge the computing resources that are provided by CERN, IN2P3 (France),

KIT and DESY (Germany), INFN (Italy), SURF (Netherlands), PIC (Spain), GridPP (United Kingdom), RRCKI and Yandex LLC (Russia), CSCS (Switzerland), IFIN-HH (Romania), CBPF (Brazil), PL-GRID (Poland) and OSC (USA). We are indebted to the communities behind the multiple open-source software packages on which we depend. Individual groups or members have received support from AvH Foundation (Germany), EPLANET, Marie Skłodowska-Curie Actions and ERC (European Union), ANR, Labex P2IO and OCEVU, and Région Auvergne-Rhône-Alpes (France), Key Research Program of Frontier Sciences of CAS, CAS PIFI, and the Thousand Talents Program (China), RFBR, RSF and Yandex LLC (Russia), GVA, XuntaGal and GENCAT (Spain), Herchel Smith Fund, the Royal Society, the English-Speaking Union and the Leverhulme Trust (United Kingdom).

References

- [1] M. Kobayashi and T. Maskawa, *CP-violation in the renormalizable theory of weak interaction*, Prog. Theor. Phys. **49** (1973) 652.
- [2] M. Dine and A. Kusenko, *The origin of the matter - antimatter asymmetry*, Rev. Mod. Phys. **76** (2003) 1, arXiv:hep-ph/0303065.
- [3] LHCb collaboration, R. Aaij *et al.*, *Measurement of CP asymmetry in $D^0 \rightarrow K^+K^-$ decays*, Phys. Lett. **B767** (2017) 177, arXiv:1610.09476.
- [4] LHCb collaboration, R. Aaij *et al.*, *Measurement of the CP violation parameter A_Γ in $D^0 \rightarrow K^+K^-$ and $D^0 \rightarrow \pi^+\pi^-$ decays*, Phys. Rev. Lett. **118** (2017) 261803, arXiv:1702.06490.
- [5] U. Nierste and S. Schacht, *CP violation in $D^0 \rightarrow K_s^0 K_s^0$* , Phys. Rev. **D92** (2015) 054036, arXiv:1508.00074.
- [6] J. Brod, A. L. Kagan, and J. Zupan, *Size of direct CP violation in singly Cabibbo-suppressed D decays*, Phys. Rev. **D86** (2012) 014023, arXiv:1111.5000.
- [7] Belle collaboration, N. Dash *et al.*, *Search for CP violation and measurement of the branching fraction in the decay $D^0 \rightarrow K_s^0 K_s^0$* , Phys. Rev. Lett. **119** (2017) 171801, arXiv:1705.05966.
- [8] LHCb collaboration, R. Aaij *et al.*, *Measurement of the time-integrated CP asymmetry in $D^0 \rightarrow K_s^0 K_s^0$ decays*, JHEP **10** (2015) 055, arXiv:1508.06087.
- [9] CLEO collaboration, G. Bonvicini *et al.*, *Search for CP violation in $D^0 \rightarrow K_s^0 \pi^0$ and $D^0 \rightarrow \pi^0 \pi^0$ and $D^0 \rightarrow K_s^0 K_s^0$ decays*, Phys. Rev. **D63** (2001) 071101, arXiv:hep-ex/0012054.
- [10] Particle Data Group, C. Patrignani *et al.*, *Review of particle physics*, Chin. Phys. **C40** (2016) 100001, and 2017 update.
- [11] LHCb collaboration, A. A. Alves Jr. *et al.*, *The LHCb detector at the LHC*, JINST **3** (2008) S08005.

- [12] LHCb collaboration, R. Aaij *et al.*, *LHCb detector performance*, Int. J. Mod. Phys. **A30** (2015) 1530022, [arXiv:1412.6352](#).
- [13] T. Sjöstrand, S. Mrenna, and P. Skands, *PYTHIA 6.4 physics and manual*, JHEP **05** (2006) 026, [arXiv:hep-ph/0603175](#); T. Sjöstrand, S. Mrenna, and P. Skands, *A brief introduction to PYTHIA 8.1*, Comput. Phys. Commun. **178** (2008) 852, [arXiv:0710.3820](#).
- [14] I. Belyaev *et al.*, *Handling of the generation of primary events in Gauss, the LHCb simulation framework*, J. Phys. Conf. Ser. **331** (2011) 032047.
- [15] D. J. Lange, *The EvtGen particle decay simulation package*, Nucl. Instrum. Meth. **A462** (2001) 152.
- [16] P. Golonka and Z. Was, *PHOTOS Monte Carlo: A precision tool for QED corrections in Z and W decays*, Eur. Phys. J. **C45** (2006) 97, [arXiv:hep-ph/0506026](#).
- [17] Geant4 collaboration, J. Allison *et al.*, *Geant4 developments and applications*, IEEE Trans. Nucl. Sci. **53** (2006) 270; Geant4 collaboration, S. Agostinelli *et al.*, *Geant4: A simulation toolkit*, Nucl. Instrum. Meth. **A506** (2003) 250.
- [18] M. Clemencic *et al.*, *The LHCb simulation application, Gauss: Design, evolution and experience*, J. Phys. Conf. Ser. **331** (2011) 032023.
- [19] I. Narsky and F. C. Porter, *Statistical analysis techniques in particle physics*, Wiley-VCH, Weinheim, Germany, 2014.
- [20] N. L. Johnson, *Systems of frequency curves generated by methods of translation*, Biometrika **36** (1949) 149.
- [21] LHCb collaboration, R. Aaij *et al.*, *Measurement of the D^\pm production asymmetry in 7 TeV pp collisions*, Phys. Lett. **B718** (2013) 902, [arXiv:1210.4112](#).
- [22] LHCb collaboration, R. Aaij *et al.*, *Measurement of the \bar{B}^0-B^0 and $\bar{B}_s^0-B_s^0$ production asymmetries in pp collisions at $\sqrt{s} = 7$ TeV*, Phys. Lett. **B739** (2014) 218, [arXiv:1408.0275](#).
- [23] LHCb collaboration, R. Aaij *et al.*, *Measurement of B^0 , B_s^0 , B^+ and Λ_b^0 production asymmetries in 7 and 8 TeV proton-proton collisions*, Phys. Lett. **B774** (2017) 139, [arXiv:1703.08464](#).
- [24] C. P. Enz and R. R. Lewis, *On the phenomenological description of CP violation for K mesons and its consequences*, Helv. Phys. Acta **38** (1965) 860.

LHCb collaboration

R. Aaij²⁷, B. Adeva⁴¹, M. Adinolfi⁴⁸, C.A. Aidala⁷³, Z. Ajaltouni⁵, S. Akar⁵⁹, P. Albicocco¹⁸, J. Albrecht¹⁰, F. Alessio⁴², M. Alexander⁵³, A. Alfonso Alberio⁴⁰, S. Ali²⁷, G. Alkhazov³³, P. Alvarez Cartelle⁵⁵, A.A. Alves Jr⁵⁹, S. Amato², S. Amerio²³, Y. Amhis⁷, L. An³, L. Anderlini¹⁷, G. Andreassi⁴³, M. Andreotti^{16,g}, J.E. Andrews⁶⁰, R.B. Appleby⁵⁶, F. Archilli²⁷, P. d'Argent¹², J. Arnau Romeu⁶, A. Artamonov³⁹, M. Artuso⁶¹, K. Arzymatov³⁷, E. Aslanides⁶, M. Atzeni⁴⁴, S. Bachmann¹², J.J. Back⁵⁰, S. Baker⁵⁵, V. Balagura^{7,b}, W. Baldini¹⁶, A. Baranov³⁷, R.J. Barlow⁵⁶, S. Barsuk⁷, W. Barter⁵⁶, F. Baryshnikov⁷⁰, V. Batozskaya³¹, B. Batsukh⁶¹, V. Battista⁴³, A. Bay⁴³, J. Beddow⁵³, F. Bedeschi²⁴, I. Bediaga¹, A. Beiter⁶¹, L.J. Bel²⁷, N. Belyi⁶³, V. Bellec⁴³, N. Belloli^{20,i}, K. Belous³⁹, I. Belyaev^{34,42}, E. Ben-Haim⁸, G. Bencivenni¹⁸, S. Benson²⁷, S. Beranek⁹, A. Berezhnoy³⁵, R. Bernet⁴⁴, D. Berninghoff¹², E. Bertholet⁸, A. Bertolin²³, C. Betancourt⁴⁴, F. Betti^{15,42}, M.O. Bettler⁴⁹, M. van Beuzekom²⁷, I.a. Bezshyiko⁴⁴, S. Bifani⁴⁷, P. Billoir⁸, A. Birnkraut¹⁰, A. Bizzeti^{17,u}, M. Björn⁵⁷, T. Blake⁵⁰, F. Blanc⁴³, S. Blusk⁶¹, D. Bobulska⁵³, V. Bocci²⁶, O. Boente Garcia⁴¹, T. Boettcher⁵⁸, A. Bondar^{38,w}, N. Bondar³³, S. Borghi^{56,42}, M. Borisyak³⁷, M. Borsato^{41,42}, F. Bossu⁷, M. Boubdir⁹, T.J.V. Bowcock⁵⁴, C. Bozzi^{16,42}, S. Braun¹², M. Brodski⁴², J. Brodzicka²⁹, D. Brundu²², E. Buchanan⁴⁸, A. Buonaura⁴⁴, C. Burr⁵⁶, A. Bursche²², J. Buytaert⁴², W. Byczynski⁴², S. Cadeddu²², H. Cai⁶⁴, R. Calabrese^{16,g}, R. Calladine⁴⁷, M. Calvi^{20,i}, M. Calvo Gomez^{40,m}, A. Camboni^{40,m}, P. Campana¹⁸, D.H. Campora Perez⁴², L. Capriotti⁵⁶, A. Carbone^{15,e}, G. Carboni²⁵, R. Cardinale^{19,h}, A. Cardini²², P. Carniti^{20,i}, L. Carson⁵², K. Carvalho Akiba², G. Casse⁵⁴, L. Cassina²⁰, M. Cattaneo⁴², G. Cavallero^{19,h}, R. Cenci^{24,p}, D. Chamont⁷, M.G. Chapman⁴⁸, M. Charles⁸, Ph. Charpentier⁴², G. Chatzikonstantinidis⁴⁷, M. Chefdeville⁴, V. Chekalina³⁷, C. Chen³, S. Chen²², S.-G. Chitic⁴², V. Chobanova⁴¹, M. Chrzaszcz⁴², A. Chubykin³³, P. Ciambrone¹⁸, X. Cid Vidal⁴¹, G. Ciezarek⁴², P.E.L. Clarke⁵², M. Clemencic⁴², H.V. Cliff⁴⁹, J. Closier⁴², V. Coco⁴², J. Cogan⁶, E. Cogneras⁵, L. Cojocariu³², P. Collins⁴², T. Colombo⁴², A. Comerma-Montells¹², A. Contu²², G. Coombs⁴², S. Coquereau⁴⁰, G. Corti⁴², M. Corvo^{16,g}, C.M. Costa Sobral⁵⁰, B. Couturier⁴², G.A. Cowan⁵², D.C. Craik⁵⁸, A. Crocombe⁵⁰, M. Cruz Torres¹, R. Currie⁵², C. D'Ambrosio⁴², F. Da Cunha Marinho², C.L. Da Silva⁷⁴, E. Dall'Occo²⁷, J. Dalseno⁴⁸, A. Danilina³⁴, A. Davis³, O. De Aguiar Francisco⁴², K. De Bruyn⁴², S. De Capua⁵⁶, M. De Cian⁴³, J.M. De Miranda¹, L. De Paula², M. De Serio^{14,d}, P. De Simone¹⁸, C.T. Dean⁵³, D. Decamp⁴, L. Del Buono⁸, B. Delaney⁴⁹, H.-P. Dembinski¹¹, M. Demmer¹⁰, A. Dendek³⁰, D. Derkach³⁷, O. Deschamps⁵, F. Dettori⁵⁴, B. Dey⁶⁵, A. Di Canto⁴², P. Di Nezza¹⁸, S. Didenko⁷⁰, H. Dijkstra⁴², F. Dordei⁴², M. Dorigo^{42,y}, A. Dosil Suárez⁴¹, L. Douglas⁵³, A. Dovbnya⁴⁵, K. Dreimanis⁵⁴, L. Dufour²⁷, G. Dujany⁸, P. Durante⁴², J.M. Durham⁷⁴, D. Dutta⁵⁶, R. Dzhelyadin³⁹, M. Dziewiecki¹², A. Dziurda⁴², A. Dzyuba³³, S. Easo⁵¹, U. Egede⁵⁵, V. Egorychev³⁴, S. Eidelman^{38,w}, S. Eisenhardt⁵², U. Eitschberger¹⁰, R. Ekelhof¹⁰, L. Eklund⁵³, S. Ely⁶¹, A. Ene³², S. Escher⁹, S. Esen²⁷, H.M. Evans⁴⁹, T. Evans⁵⁷, A. Falabella¹⁵, N. Farley⁴⁷, S. Farry⁵⁴, D. Fazzini^{20,42,i}, L. Federici²⁵, G. Fernandez⁴⁰, P. Fernandez Declara⁴², A. Fernandez Prieto⁴¹, F. Ferrari¹⁵, L. Ferreira Lopes⁴³, F. Ferreira Rodrigues², M. Ferro-Luzzi⁴², S. Filippov³⁶, R.A. Fini¹⁴, M. Fiorini^{16,g}, M. Firlej³⁰, C. Fitzpatrick⁴³, T. Fiutowski³⁰, F. Fleuret^{7,b}, M. Fontana^{22,42}, F. Fontanelli^{19,h}, R. Forty⁴², V. Franco Lima⁵⁴, M. Frank⁴², C. Frei⁴², J. Fu^{21,q}, W. Funk⁴², C. Färber⁴², M. Féo Pereira Rivello Carvalho²⁷, E. Gabriel⁵², A. Gallas Torreira⁴¹, D. Galli^{15,e}, S. Gallorini²³, S. Gambetta⁵², M. Gandelman², P. Gandini²¹, Y. Gao³, L.M. Garcia Martin⁷², B. Garcia Plana⁴¹, J. García Pardiñas⁴⁴, J. Garra Tico⁴⁹, L. Garrido⁴⁰, D. Gascon⁴⁰, C. Gaspar⁴², L. Gavardi¹⁰, G. Gazzoni⁵, D. Gerick¹², E. Gersabeck⁵⁶, M. Gersabeck⁵⁶, T. Gershon⁵⁰, Ph. Ghez⁴, S. Gianì⁴³, V. Gibson⁴⁹, O.G. Girard⁴³, L. Giubega³², K. Gizdov⁵², V.V. Gligorov⁸, D. Golubkov³⁴, A. Golutvin^{55,70}, A. Gomes^{1,a}, I.V. Gorelov³⁵, C. Gotti^{20,i}, E. Govorkova²⁷, J.P. Grabowski¹², R. Graciani Diaz⁴⁰, L.A. Granado Cardoso⁴², E. Graugés⁴⁰,

E. Graverini⁴⁴, G. Graziani¹⁷, A. Grecu³², R. Greim²⁷, P. Griffith²², L. Grillo⁵⁶, L. Gruber⁴²,
 B.R. Gruberg Cazon⁵⁷, O. Grünberg⁶⁷, C. Gu³, E. Gushchin³⁶, Yu. Guz^{39,42}, T. Gys⁴²,
 C. Göbel⁶², T. Hadavizadeh⁵⁷, C. Hadjivasiliou⁵, G. Haefeli⁴³, C. Haen⁴², S.C. Haines⁴⁹,
 B. Hamilton⁶⁰, X. Han¹², T.H. Hancock⁵⁷, S. Hansmann-Menzemer¹², N. Harnew⁵⁷,
 S.T. Harnew⁴⁸, C. Hasse⁴², M. Hatch⁴², J. He⁶³, M. Hecker⁵⁵, K. Heinicke¹⁰, A. Heister⁹,
 K. Hennessy⁵⁴, L. Henry⁷², E. van Herwijnen⁴², M. Heß⁶⁷, A. Hicheur², D. Hill⁵⁷, M. Hilton⁵⁶,
 P.H. Hopchev⁴³, W. Hu⁶⁵, W. Huang⁶³, Z.C. Huard⁵⁹, W. Hulsbergen²⁷, T. Humair⁵⁵,
 M. Hushchyn³⁷, D. Hutchcroft⁵⁴, D. Hynds²⁷, P. Ibis¹⁰, M. Idzik³⁰, P. Ilten⁴⁷, K. Ivshin³³,
 R. Jacobsson⁴², J. Jalocha⁵⁷, E. Jans²⁷, A. Jawahery⁶⁰, F. Jiang³, M. John⁵⁷, D. Johnson⁴²,
 C.R. Jones⁴⁹, C. Joram⁴², B. Jost⁴², N. Jurik⁵⁷, S. Kandybei⁴⁵, M. Karacson⁴², J.M. Kariuki⁴⁸,
 S. Karodia⁵³, N. Kazeev³⁷, M. Kecke¹², F. Keizer⁴⁹, M. Kelsey⁶¹, M. Kenzie⁴⁹, T. Ketel²⁸,
 E. Khairullin³⁷, B. Khanji¹², C. Khurewathanakul⁴³, K.E. Kim⁶¹, T. Kirn⁹, S. Klaver¹⁸,
 K. Klimaszewski³¹, T. Klimkovich¹¹, S. Koliiev⁴⁶, M. Kolpin¹², R. Kopečna¹², P. Koppenburg²⁷,
 S. Kotriakhova³³, M. Kozeiha⁵, L. Kravchuk³⁶, M. Kreps⁵⁰, F. Kress⁵⁵, P. Krokovny^{38,w},
 W. Krupa³⁰, W. Krzemien³¹, W. Kucewicz^{29,l}, M. Kucharczyk²⁹, V. Kudryavtsev^{38,w},
 A.K. Kuonen⁴³, T. Kvaratskheliya^{34,42}, D. Lacarrere⁴², G. Lafferty⁵⁶, A. Lai²², D. Lancierini⁴⁴,
 G. Lanfranchi¹⁸, C. Langenbruch⁹, T. Latham⁵⁰, C. Lazzeroni⁴⁷, R. Le Gac⁶, A. Leflat³⁵,
 J. Lefrançois⁷, R. Lefèvre⁵, F. Lemaître⁴², O. Leroy⁶, T. Lesiak²⁹, B. Leverington¹², P.-R. Li⁶³,
 T. Li³, Z. Li⁶¹, X. Liang⁶¹, T. Likhomanenko⁶⁹, R. Lindner⁴², F. Lionetto⁴⁴, V. Lisovskyi⁷,
 X. Liu³, D. Loh⁵⁰, A. Loi²², I. Longstaff⁵³, J.H. Lopes², D. Lucchesi^{23,o}, M. Lucio Martinez⁴¹,
 A. Lupato²³, E. Luppi^{16,g}, O. Lupton⁴², A. Lusiani²⁴, X. Lyu⁶³, F. Machefert⁷, F. Maciuc³²,
 V. Macko⁴³, P. Mackowiak¹⁰, S. Maddrell-Mander⁴⁸, O. Maev^{33,42}, K. Maguire⁵⁶,
 D. Maisuzenko³³, M.W. Majewski³⁰, S. Malde⁵⁷, B. Malecki²⁹, A. Malinin⁶⁹, T. Maltsev^{38,w},
 G. Manca^{22,f}, G. Mancinelli⁶, D. Marangotto^{21,q}, J. Maratas^{5,v}, J.F. Marchand⁴, U. Marconi¹⁵,
 C. Marin Benito⁴⁰, M. Marinangeli⁴³, P. Marino⁴³, J. Marks¹², G. Martellotti²⁶, M. Martin⁶,
 M. Martinelli⁴³, D. Martinez Santos⁴¹, F. Martinez Vidal⁷², A. Massafferri¹, R. Matev⁴²,
 A. Mathad⁵⁰, Z. Mathe⁴², C. Matteuzzi²⁰, A. Mauri⁴⁴, E. Maurice^{7,b}, B. Maurin⁴³,
 A. Mazurov⁴⁷, M. McCann^{55,42}, A. McNab⁵⁶, R. McNulty¹³, J.V. Mead⁵⁴, B. Meadows⁵⁹,
 C. Meaux⁶, F. Meier¹⁰, N. Meinert⁶⁷, D. Melnychuk³¹, M. Merk²⁷, A. Merli^{21,q}, E. Michielin²³,
 D.A. Milanese⁶⁶, E. Millard⁵⁰, M.-N. Minard⁴, L. Minzoni^{16,g}, D.S. Mitzel¹², A. Mogini⁸,
 J. Molina Rodriguez^{1,z}, T. Mombächer¹⁰, I.A. Monroy⁶⁶, S. Monteil⁵, M. Morandin²³,
 G. Morello¹⁸, M.J. Morello^{24,t}, O. Morgunova⁶⁹, J. Moron³⁰, A.B. Morris⁶, R. Mountain⁶¹,
 F. Muheim⁵², M. Mulder²⁷, D. Müller⁴², J. Müller¹⁰, K. Müller⁴⁴, V. Müller¹⁰, P. Naik⁴⁸,
 T. Nakada⁴³, R. Nandakumar⁵¹, A. Nandi⁵⁷, T. Nanut⁴³, I. Nasteva², M. Needham⁵², N. Neri²¹,
 S. Neubert¹², N. Neufeld⁴², M. Neuner¹², T.D. Nguyen⁴³, C. Nguyen-Mau^{43,n}, S. Nieswand⁹,
 R. Niet¹⁰, N. Nikitin³⁵, A. Nogay⁶⁹, D.P. O'Hanlon¹⁵, A. Oblakowska-Mucha³⁰, V. Obraztsov³⁹,
 S. Ogilvy¹⁸, R. Oldeman^{22,f}, C.J.G. Onderwater⁶⁸, A. Ossowska²⁹, J.M. Otalora Goicochea²,
 P. Owen⁴⁴, A. Oyanguren⁷², P.R. Pais⁴³, A. Palano¹⁴, M. Palutan^{18,42}, G. Panshin⁷¹,
 A. Papanestis⁵¹, M. Pappagallo⁵², L.L. Pappalardo^{16,g}, W. Parker⁶⁰, C. Parkes⁵⁶,
 G. Passaleva^{17,42}, A. Pastore¹⁴, M. Patel⁵⁵, C. Patrignani^{15,e}, A. Pearce⁴², A. Pellegrino²⁷,
 G. Penso²⁶, M. Pepe Altarelli⁴², S. Perazzini⁴², D. Pereima³⁴, P. Perret⁵, L. Pescatore⁴³,
 K. Petridis⁴⁸, A. Petrolini^{19,h}, A. Petrov⁶⁹, M. Petruzzo^{21,q}, B. Pietrzyk⁴, G. Pietrzyk⁴³,
 M. Pikies²⁹, D. Pinci²⁶, J. Pinzino⁴², F. Pisani⁴², A. Pistone^{19,h}, A. Piucci¹², V. Placinta³²,
 S. Playfer⁵², J. Plews⁴⁷, M. Plo Casasus⁴¹, F. Polci⁸, M. Poli Lener¹⁸, A. Poluektov⁵⁰,
 N. Polukhina^{70,c}, I. Polyakov⁶¹, E. Polcarpo², G.J. Pomery⁴⁸, S. Ponce⁴², A. Popov³⁹,
 D. Popov^{47,11}, S. Poslavskii³⁹, C. Potterat², E. Price⁴⁸, J. Prisciandaro⁴¹, C. Prouve⁴⁸,
 V. Pugatch⁴⁶, A. Puig Navarro⁴⁴, H. Pullen⁵⁷, G. Punzi^{24,p}, W. Qian⁶³, J. Qin⁶³, R. Quagliani⁸,
 B. Quintana⁵, B. Rachwal³⁰, J.H. Rademacker⁴⁸, M. Rama²⁴, M. Ramos Pernas⁴¹, M.S. Rangel²,
 F. Ratnikov^{37,x}, G. Raven²⁸, M. Ravonel Salzgeber⁴², M. Reboud⁴, F. Redi⁴³, S. Reichert¹⁰,
 A.C. dos Reis¹, F. Reiss⁸, C. Remon Alepuz⁷², Z. Ren³, V. Renaudin⁷, S. Ricciardi⁵¹,

S. Richards⁴⁸, K. Rinnert⁵⁴, P. Robbe⁷, A. Robert⁸, A.B. Rodrigues⁴³, E. Rodrigues⁵⁹, J.A. Rodriguez Lopez⁶⁶, A. Rogozhnikov³⁷, S. Roiser⁴², A. Rollings⁵⁷, V. Romanovskiy³⁹, A. Romero Vidal⁴¹, M. Rotondo¹⁸, M.S. Rudolph⁶¹, T. Ruf⁴², J. Ruiz Vidal⁷², J.J. Saborido Silva⁴¹, N. Sagidova³³, B. Saitta^{22,f}, V. Salustino Guimaraes⁶², C. Sanchez Gras²⁷, C. Sanchez Mayordomo⁷², B. Sanmartin Sedes⁴¹, R. Santacesaria²⁶, C. Santamarina Rios⁴¹, M. Santimaria¹⁸, E. Santovetti^{25,j}, G. Sarpis⁵⁶, A. Sarti^{18,k}, C. Satriano^{26,s}, A. Satta²⁵, M. Saur⁶³, D. Savrina^{34,35}, S. Schael⁹, M. Schellenberg¹⁰, M. Schiller⁵³, H. Schindler⁴², M. Schmelling¹¹, T. Schmelzer¹⁰, B. Schmidt⁴², O. Schneider⁴³, A. Schopper⁴², H.F. Schreiner⁵⁹, M. Schubiger⁴³, M.H. Schune⁷, R. Schwemmer⁴², B. Sciascia¹⁸, A. Sciubba^{26,k}, A. Semennikov³⁴, E.S. Sepulveda⁸, A. Sergi^{47,42}, N. Serra⁴⁴, J. Serrano⁶, L. Sestini²³, P. Seyfert⁴², M. Shapkin³⁹, Y. Shcheglov^{33,†}, T. Shears⁵⁴, L. Shekhtman^{38,w}, V. Shevchenko⁶⁹, E. Shmanin⁷⁰, B.G. Siddi¹⁶, R. Silva Coutinho⁴⁴, L. Silva de Oliveira², G. Simi^{23,o}, S. Simone^{14,d}, N. Skidmore¹², T. Skwarnicki⁶¹, E. Smith⁹, I.T. Smith⁵², M. Smith⁵⁵, M. Soares¹⁵, I. Soares Lavra¹, M.D. Sokoloff⁵⁹, F.J.P. Soler⁵³, B. Souza De Paula², B. Spaan¹⁰, P. Spradlin⁵³, F. Stagni⁴², M. Stahl¹², S. Stahl⁴², P. Stefko⁴³, S. Stefkova⁵⁵, O. Steinkamp⁴⁴, S. Stemmler¹², O. Stenyakin³⁹, M. Stepanova³³, H. Stevens¹⁰, S. Stone⁶¹, B. Storaci⁴⁴, S. Stracka²⁴, M.E. Stramaglia⁴³, M. Straticiu³², U. Straumann⁴⁴, S. Strovov⁷¹, J. Sun³, L. Sun⁶⁴, K. Swientek³⁰, V. Syropoulos²⁸, T. Szumlak³⁰, M. Szymanski⁶³, S. T'Jampens⁴, Z. Tang³, A. Tayduganov⁶, T. Tekampe¹⁰, G. Tellarini¹⁶, F. Teubert⁴², E. Thomas⁴², J. van Tilburg²⁷, M.J. Tilley⁵⁵, V. Tisserand⁵, M. Tobin⁴³, S. Tolc⁴², L. Tomassetti^{16,g}, D. Tonelli²⁴, D.Y. Tou⁸, R. Tourinho Jadallah Aoude¹, E. Tournefier⁴, M. Traill⁵³, M.T. Tran⁴³, A. Trisovic⁴⁹, A. Tsaregorodtsev⁶, G. Tuci^{24,p}, A. Tully⁴⁹, N. Tuning^{27,42}, A. Ukleja³¹, A. Usachov⁷, A. Ustyuzhanin³⁷, U. Uwer¹², C. Vacca^{22,f}, A. Vagner⁷¹, V. Vagnoni¹⁵, A. Valassi⁴², S. Valat⁴², G. Valenti¹⁵, R. Vazquez Gomez⁴², P. Vazquez Regueiro⁴¹, S. Vecchi¹⁶, M. van Veghel²⁷, J.J. Velthuis⁴⁸, M. Veltri^{17,r}, G. Veneziano⁵⁷, A. Venkateswaran⁶¹, T.A. Verlage⁹, M. Vernet⁵, M. Vesterinen⁵⁷, J.V. Viana Barbosa⁴², D. Vieira⁶³, M. Vieites Diaz⁴¹, H. Viemann⁶⁷, X. Vilasis-Cardona^{40,m}, A. Vitkovskiy²⁷, M. Vitti⁴⁹, V. Volkov³⁵, A. Vollhardt⁴⁴, B. Voneki⁴², A. Vorobyev³³, V. Vorobyev^{38,w}, C. Voß⁹, J.A. de Vries²⁷, C. Vázquez Sierra²⁷, R. Waldi⁶⁷, J. Walsh²⁴, J. Wang⁶¹, M. Wang³, Y. Wang⁶⁵, Z. Wang⁴⁴, D.R. Ward⁴⁹, H.M. Wark⁵⁴, N.K. Watson⁴⁷, D. Websdale⁵⁵, A. Weiden⁴⁴, C. Weisser⁵⁸, M. Whitehead⁹, J. Wicht⁵⁰, G. Wilkinson⁵⁷, M. Wilkinson⁶¹, M.R.J. Williams⁵⁶, M. Williams⁵⁸, T. Williams⁴⁷, F.F. Wilson^{51,42}, J. Wimberley⁶⁰, M. Winn⁷, J. Wishahi¹⁰, W. Wislicki³¹, M. Witek²⁹, G. Wormser⁷, S.A. Wotton⁴⁹, K. Wyllie⁴², D. Xiao⁶⁵, Y. Xie⁶⁵, A. Xu³, M. Xu⁶⁵, Q. Xu⁶³, Z. Xu³, Z. Xu⁴, Z. Yang³, Z. Yang⁶⁰, Y. Yao⁶¹, H. Yin⁶⁵, J. Yu^{65,ab}, X. Yuan⁶¹, O. Yushchenko³⁹, K.A. Zarebski⁴⁷, M. Zavertyaev^{11,c}, D. Zhang⁶⁵, L. Zhang³, W.C. Zhang^{3,aa}, Y. Zhang⁷, A. Zhelezov¹², Y. Zheng⁶³, X. Zhu³, V. Zhukov^{9,35}, J.B. Zonneveld⁵², S. Zucchelli¹⁵.

¹Centro Brasileiro de Pesquisas Físicas (CBPF), Rio de Janeiro, Brazil

²Universidade Federal do Rio de Janeiro (UFRJ), Rio de Janeiro, Brazil

³Center for High Energy Physics, Tsinghua University, Beijing, China

⁴Univ. Grenoble Alpes, Univ. Savoie Mont Blanc, CNRS, IN2P3-LAPP, Annecy, France

⁵Clermont Université, Université Blaise Pascal, CNRS/IN2P3, LPC, Clermont-Ferrand, France

⁶Aix Marseille Univ, CNRS/IN2P3, CPPM, Marseille, France

⁷LAL, Univ. Paris-Sud, CNRS/IN2P3, Université Paris-Saclay, Orsay, France

⁸LPNHE, Sorbonne Université, Paris Diderot Sorbonne Paris Cité, CNRS/IN2P3, Paris, France

⁹I. Physikalisches Institut, RWTH Aachen University, Aachen, Germany

¹⁰Fakultät Physik, Technische Universität Dortmund, Dortmund, Germany

¹¹Max-Planck-Institut für Kernphysik (MPIK), Heidelberg, Germany

¹²Physikalisches Institut, Ruprecht-Karls-Universität Heidelberg, Heidelberg, Germany

¹³School of Physics, University College Dublin, Dublin, Ireland

¹⁴INFN Sezione di Bari, Bari, Italy

¹⁵INFN Sezione di Bologna, Bologna, Italy

- ¹⁶ *INFN Sezione di Ferrara, Ferrara, Italy*
- ¹⁷ *INFN Sezione di Firenze, Firenze, Italy*
- ¹⁸ *INFN Laboratori Nazionali di Frascati, Frascati, Italy*
- ¹⁹ *INFN Sezione di Genova, Genova, Italy*
- ²⁰ *INFN Sezione di Milano-Bicocca, Milano, Italy*
- ²¹ *INFN Sezione di Milano, Milano, Italy*
- ²² *INFN Sezione di Cagliari, Monserrato, Italy*
- ²³ *INFN Sezione di Padova, Padova, Italy*
- ²⁴ *INFN Sezione di Pisa, Pisa, Italy*
- ²⁵ *INFN Sezione di Roma Tor Vergata, Roma, Italy*
- ²⁶ *INFN Sezione di Roma La Sapienza, Roma, Italy*
- ²⁷ *Nikhef National Institute for Subatomic Physics, Amsterdam, Netherlands*
- ²⁸ *Nikhef National Institute for Subatomic Physics and VU University Amsterdam, Amsterdam, Netherlands*
- ²⁹ *Henryk Niewodniczanski Institute of Nuclear Physics Polish Academy of Sciences, Kraków, Poland*
- ³⁰ *AGH - University of Science and Technology, Faculty of Physics and Applied Computer Science, Kraków, Poland*
- ³¹ *National Center for Nuclear Research (NCBJ), Warsaw, Poland*
- ³² *Horia Hulubei National Institute of Physics and Nuclear Engineering, Bucharest-Magurele, Romania*
- ³³ *Petersburg Nuclear Physics Institute (PNPI), Gatchina, Russia*
- ³⁴ *Institute of Theoretical and Experimental Physics (ITEP), Moscow, Russia*
- ³⁵ *Institute of Nuclear Physics, Moscow State University (SINP MSU), Moscow, Russia*
- ³⁶ *Institute for Nuclear Research of the Russian Academy of Sciences (INR RAS), Moscow, Russia*
- ³⁷ *Yandex School of Data Analysis, Moscow, Russia*
- ³⁸ *Budker Institute of Nuclear Physics (SB RAS), Novosibirsk, Russia*
- ³⁹ *Institute for High Energy Physics (IHEP), Protvino, Russia*
- ⁴⁰ *ICCUB, Universitat de Barcelona, Barcelona, Spain*
- ⁴¹ *Instituto Galego de Física de Altas Enerxías (IGFAE), Universidade de Santiago de Compostela, Santiago de Compostela, Spain*
- ⁴² *European Organization for Nuclear Research (CERN), Geneva, Switzerland*
- ⁴³ *Institute of Physics, Ecole Polytechnique Fédérale de Lausanne (EPFL), Lausanne, Switzerland*
- ⁴⁴ *Physik-Institut, Universität Zürich, Zürich, Switzerland*
- ⁴⁵ *NSC Kharkiv Institute of Physics and Technology (NSC KIPT), Kharkiv, Ukraine*
- ⁴⁶ *Institute for Nuclear Research of the National Academy of Sciences (KINR), Kyiv, Ukraine*
- ⁴⁷ *University of Birmingham, Birmingham, United Kingdom*
- ⁴⁸ *H.H. Wills Physics Laboratory, University of Bristol, Bristol, United Kingdom*
- ⁴⁹ *Cavendish Laboratory, University of Cambridge, Cambridge, United Kingdom*
- ⁵⁰ *Department of Physics, University of Warwick, Coventry, United Kingdom*
- ⁵¹ *STFC Rutherford Appleton Laboratory, Didcot, United Kingdom*
- ⁵² *School of Physics and Astronomy, University of Edinburgh, Edinburgh, United Kingdom*
- ⁵³ *School of Physics and Astronomy, University of Glasgow, Glasgow, United Kingdom*
- ⁵⁴ *Oliver Lodge Laboratory, University of Liverpool, Liverpool, United Kingdom*
- ⁵⁵ *Imperial College London, London, United Kingdom*
- ⁵⁶ *School of Physics and Astronomy, University of Manchester, Manchester, United Kingdom*
- ⁵⁷ *Department of Physics, University of Oxford, Oxford, United Kingdom*
- ⁵⁸ *Massachusetts Institute of Technology, Cambridge, MA, United States*
- ⁵⁹ *University of Cincinnati, Cincinnati, OH, United States*
- ⁶⁰ *University of Maryland, College Park, MD, United States*
- ⁶¹ *Syracuse University, Syracuse, NY, United States*
- ⁶² *Pontifícia Universidade Católica do Rio de Janeiro (PUC-Rio), Rio de Janeiro, Brazil, associated to ²*
- ⁶³ *University of Chinese Academy of Sciences, Beijing, China, associated to ³*
- ⁶⁴ *School of Physics and Technology, Wuhan University, Wuhan, China, associated to ³*
- ⁶⁵ *Institute of Particle Physics, Central China Normal University, Wuhan, Hubei, China, associated to ³*
- ⁶⁶ *Departamento de Física, Universidad Nacional de Colombia, Bogota, Colombia, associated to ⁸*
- ⁶⁷ *Institut für Physik, Universität Rostock, Rostock, Germany, associated to ¹²*
- ⁶⁸ *Van Swinderen Institute, University of Groningen, Groningen, Netherlands, associated to ²⁷*

- ⁶⁹ *National Research Centre Kurchatov Institute, Moscow, Russia, associated to* ³⁴
⁷⁰ *National University of Science and Technology "MISIS", Moscow, Russia, associated to* ³⁴
⁷¹ *National Research Tomsk Polytechnic University, Tomsk, Russia, associated to* ³⁴
⁷² *Instituto de Fisica Corpuscular, Centro Mixto Universidad de Valencia - CSIC, Valencia, Spain, associated to* ⁴⁰
⁷³ *University of Michigan, Ann Arbor, United States, associated to* ⁶¹
⁷⁴ *Los Alamos National Laboratory (LANL), Los Alamos, United States, associated to* ⁶¹

- ^a *Universidade Federal do Triângulo Mineiro (UFTM), Uberaba-MG, Brazil*
^b *Laboratoire Leprince-Ringuet, Palaiseau, France*
^c *P.N. Lebedev Physical Institute, Russian Academy of Science (LPI RAS), Moscow, Russia*
^d *Università di Bari, Bari, Italy*
^e *Università di Bologna, Bologna, Italy*
^f *Università di Cagliari, Cagliari, Italy*
^g *Università di Ferrara, Ferrara, Italy*
^h *Università di Genova, Genova, Italy*
ⁱ *Università di Milano Bicocca, Milano, Italy*
^j *Università di Roma Tor Vergata, Roma, Italy*
^k *Università di Roma La Sapienza, Roma, Italy*
^l *AGH - University of Science and Technology, Faculty of Computer Science, Electronics and Telecommunications, Kraków, Poland*
^m *LIFAEELS, La Salle, Universitat Ramon Llull, Barcelona, Spain*
ⁿ *Hanoi University of Science, Hanoi, Vietnam*
^o *Università di Padova, Padova, Italy*
^p *Università di Pisa, Pisa, Italy*
^q *Università degli Studi di Milano, Milano, Italy*
^r *Università di Urbino, Urbino, Italy*
^s *Università della Basilicata, Potenza, Italy*
^t *Scuola Normale Superiore, Pisa, Italy*
^u *Università di Modena e Reggio Emilia, Modena, Italy*
^v *MSU - Iligan Institute of Technology (MSU-IIT), Iligan, Philippines*
^w *Novosibirsk State University, Novosibirsk, Russia*
^x *National Research University Higher School of Economics, Moscow, Russia*
^y *Sezione INFN di Trieste, Trieste, Italy*
^z *Escuela Agrícola Panamericana, San Antonio de Oriente, Honduras*
^{aa} *School of Physics and Information Technology, Shaanxi Normal University (SNNU), Xi'an, China*
^{ab} *Physics and Micro Electronic College, Hunan University, Changsha City, China*

† *Deceased*